Scientific Reports

https://doi.org/10.1038/s41598-026-62081-6

Article in Press

A green electrochemical sensor based on Fe/N-graphene hybrid nanostructure for trace-level determination of apremilast in biological and pharmaceutical samples

Received: 30 March 2026

Accepted: 9 July 2026

Published online: 15 July 2026

Cite this article as: Naser M., Bouali W., Karaman O. *et al.* A green electrochemical sensor based on Fe/N-graphene hybrid nanostructure for trace-level determination of apremilast in biological and pharmaceutical samples. *Sci Rep* (2026). https://doi.org/10.1038/s41598-026-62081-6

Marwah Naser, Wiem Bouali, Onur Karaman, Pedro Gómez-Romero, Ceren Karaman & Nevin Erk

We are providing an unedited version of this manuscript to give early access to its findings. Before final publication, the manuscript will undergo further editing. Please note there may be errors present which affect the content, and all legal disclaimers apply.

If this paper is publishing under a Transparent Peer Review model then Peer Review reports will publish with the final article.

ARTICLE IN PRESS

© The Author(s) 2026. **Open Access** This article is licensed under a Creative Commons Attribution-NonCommercial-NoDerivatives 4.0 International License, which permits any non-commercial use, sharing, distribution and reproduction in any medium or format, as long as you give appropriate credit to the original author(s) and the source, provide a link to the Creative Commons licence, and indicate if you modified the licensed material. You do not have permission under this licence to share adapted material derived from this article or parts of it. The images or other third party material in this article are included in the article's Creative Commons licence, unless indicated otherwise in a credit line to the material. If material is not included in the article's Creative Commons licence and your intended use is not permitted by statutory regulation or exceeds the permitted use, you will need to obtain permission directly from the copyright holder. To view a copy of this licence, visit http://creativecommons.org/licenses/by-nc-nd/4.0/.

ARTICLE IN PRESS

A Green Electrochemical Sensor Based on Fe/N-Graphene Hybrid Nanostructure for Trace-Level Determination of Apremilast in Biological and Pharmaceutical Samples

Marwah Naser[a], Wiem Bouali[a], Onur Karaman[b], Pedro Gómez-Romero[c], Ceren Karaman[d,c*], Nevin Erk[a*]

[a]*Ankara University, Faculty of Pharmacy, Department of Analytical Chemistry, 06560 Ankara, Turkey*

[b]*Akdeniz University, Department of Medical Imaging Techniques, Antalya, Turkey*

[c]*ICN2 (Catalan Institute of Nanoscience and Nanotechnology), and The Barcelona Institute of Science and Technology (CSIC-BIST), Campus UAB, Bellaterra, 08193, Barcelona, Spain*

[d]*Akdeniz University, Electricity and Energy Department, 07070 Antalya, Turkey*

ARTICLE IN PRESS

***Corresponding authors' emails**

cerenkaraman@akdeniz.edu.tr (C. Karaman), erk@pharmacy.ankara.edu.tr (N. Erk)

ARTICLE IN PRESS

Abstract

A Fe-containing N-doped graphene nanosheet-modified glassy carbon electrode (Fe/N-Gr/GCE) was developed for the sensitive electrochemical determination of apremilast (APRE), a phosphodiesterase-4 inhibitor used in the treatment of psoriatic arthritis. The electrochemical response of APRE was investigated using differential pulse voltammetry (DPV), showing a well-defined oxidation peak in Britton-Robinson buffer (pH 2.0). The enhanced performance of the sensor is attributed to the high surface area and favorable electron-transfer properties of the Fe/N-Gr nanomaterial. Under optimized conditions, a linear range of 0.1-22.0 μM (R^2 = 0.998) was obtained, with a detection limit of 0.008 μM and a quantification limit of 0.029 μM. The sensor exhibited good repeatability (RSD = 2.4%) and reproducibility (RSD = 2.1%), confirming its precision and fabrication reliability. Its applicability was demonstrated in synthetic human serum, urine, and pharmaceutical tablets, with recoveries of 97.41-102.71% and RSDs of 1.25-2.36%. Overall, the proposed method offers a simple, sensitive, and environmentally friendly approach for APRE determination in pharmaceutical and biological samples.

ARTICLE IN PRESS

Keywords: Apremilast; N-doped graphene nanosheets; iron-modified graphene; Pharmaceutical sample; Electrochemical sensor; Differential pulse voltammetry; Modified electrode; Biological and pharmaceutical analysis

ARTICLE IN PRESS

1. Introduction

Psoriatic arthritis is a chronic, immune-mediated inflammatory joint disease that develops in approximately one-third of individuals with psoriasis, affecting nearly 0.3-1.0% of the global population [1]. It is characterized by progressive joint inflammation, pain, and functional impairment, often accompanied by systemic inflammatory manifestations. Although several pharmacological treatment options are available, including non-steroidal anti-inflammatory drugs, disease-modifying antirheumatic drugs, and biologic agents, a significant proportion of patients experience inadequate therapeutic response, reduced long-term efficacy, or treatment-limiting adverse effects. These limitations have driven the development of alternative orally administered therapies targeting specific molecular pathways involved in inflammatory regulation [2].

Apremilast (APRE) (Figure 1) is an orally administered small-molecule drug that selectively inhibits phosphodiesterase-4 (PDE4), a key intracellular enzyme involved in the regulation of inflammatory signaling pathways [3]. Inhibition of PDE4 leads to elevated intracellular cAMP levels, resulting in downregulation of pro-inflammatory mediators (e.g., TNF-α, IL-17, IL-23) and upregulation of anti-inflammatory cytokines. Through this mechanism, APRE modulates immune responses without direct immunosuppression [4]. Owing to its favorable efficacy and safety profile, APRE has emerged as an important therapeutic option for immune-mediated inflammatory disorders. Clinical investigations, including Phase II and III trials, have demonstrated its efficacy in patients with moderate to severe plaque psoriasis, active psoriatic arthritis, and Behçet's disease [5]. Based on these results, APRE was approved by the U.S. Food and Drug Administration in 2014 for

ARTICLE IN PRESS

the treatment of adults with active psoriatic arthritis and is now widely used as an oral therapy for psoriasis-related inflammatory conditions [6].

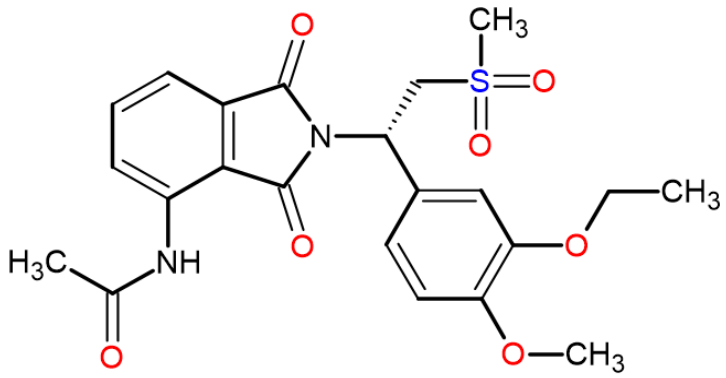


Figure 1. Chemical structure of Apremilast

Accurate determination of APRE is essential for pharmaceutical quality control, dosage verification, and therapeutic monitoring. Variations in drug concentration may affect therapeutic efficacy and patient safety, especially during long-term treatment. Therefore, developing sensitive and reliable analytical methods for APRE quantification in pharmaceutical and biological samples remains important [4].

To date, numerous studies have explored the quantification of APRE in different matrices through diverse analytical methodologies, including the UV-Spectrophotometric method [7], ultra-performance liquid chromatography coupled with tandem mass spectrometry (UPLC-MS/MS) [2], [8], high-performance liquid chromatography (HPLC), and reversed-phase HPLC with photodiode array detection (RP-HPLC)-PDA [4]. Although these conventional techniques offer high sensitivity and accuracy, their routine application is often limited by laborious and multistep sample preparation, high consumption of organic

ARTICLE IN PRESS

solvents and reagents, expensive instrumentation, extended analysis times, and the need for skilled personnel [9].

In recent years, electrochemical sensors have gained considerable attention owing to advances in nanostructured electrode materials, surface engineering, and signal-transduction strategies [10]. Compared with conventional analytical techniques, electrochemical sensing platforms offer high sensitivity, operational simplicity, rapid response, low cost, and minimal sample consumption. Moreover, electrochemical sensors are readily adaptable to portable and miniaturized formats, and their analytical performance can be rationally tuned through electrode surface modification and the incorporation of functional nanomaterials, making them particularly attractive for pharmaceutical and clinical analysis [11].

Among electroanalytical techniques, differential pulse voltammetry (DPV) is widely recognized as a sensitive and selective electroanalytical technique for the investigation of electroactive species [12]. The method employs a sequence of potential pulses superimposed on a linear potential ramp, which effectively minimizes the non-faradaic (capacitive) background current while selectively amplifying the faradaic response. This results in enhanced signal-to-noise ratios and significantly lower detection limits. Consequently, DPV enables accurate and precise quantification of analytes at trace concentration levels, rendering it particularly suitable for applications in pharmaceutical analysis, biomedical diagnostics, and environmental monitoring. Moreover, its operational simplicity, low instrumental cost, and compatibility with miniaturized and portable sensing platforms make DPV an attractive technique for routine analytical determinations requiring high reproducibility and reliability [13]. Complementarily, cyclic voltammetry (CV)

ARTICLE IN PRESS

is extensively employed to investigate electrochemical behavior, redox mechanisms, electron-transfer kinetics, and mass-transport phenomena, as well as to evaluate the effects of electrode surface modification [14].

Electrode surface engineering plays a pivotal role in advancing electrochemical sensor performance [15]. The introduction of nanostructured and heteroatom-functionalized materials significantly enhances charge-transfer efficiency, increases the density of electroactive sites, and improves analyte adsorption and interfacial interactions. These effects collectively contribute to lower detection limits, improved selectivity, and greater analytical stability, extending the applicability of electrochemical sensors to real biological and pharmaceutical samples [16].

Glassy carbon electrodes (GCEs) are widely used in electroanalysis due to their broad potential window, low background current, chemical inertness, and good mechanical stability. However, bare GCEs often exhibit limited sensitivity toward complex organic molecules, requiring surface modification to improve their electroanalytical performance. In this context, graphene (Gr) has emerged as a promising material for electrode design owing to its excellent structural, mechanical, and electrical properties. Its high specific surface area and electrical conductivity enable efficient charge transport and rapid electron-transfer processes, making it suitable for electrochemical applications [17].

Graphene and its derivatives can be synthesized using various approaches, including chemical vapor deposition, self-assembly, spin coating, vacuum filtration, thermal decomposition, and solution-based techniques [8, 10-15], which enable the fabrication of composites with tunable chemical properties. The incorporation of heteroatoms such as nitrogen into the graphene lattice further enhances electronic properties, introduces

ARTICLE IN PRESS

defect-induced active sites, and improves analyte-electrode interactions. Incorporation of iron species into N-doped graphene architectures offers additional advantages for electrochemical sensing [18]. Iron-containing domains may contribute to improved interfacial charge transfer, while their association with nitrogen-functionalized graphene can enhance surface interactions and electrochemical responsiveness [19]. Iron-containing graphene architectures have also attracted attention owing to their chemical and biological stability, low toxicity, and favorable electrochemical properties. In addition, their high electrical conductivity and intrinsic electrocatalytic activity enable efficient electron transport, allowing them to function as effective electronic mediators that enhance interfacial electron-transfer processes [20].

The synergistic combination of Fe species with N-doped graphene thus enables signal amplification through increased electroactive surface area, improved adsorption of electroactive molecules, and accelerated electron-transfer kinetics, all of which are essential for sensitive electrochemical detection [21] [22].

Recent progress in electrochemical sensors has focused on carbon-based materials such as multi-walled carbon nanotubes (MWCNTs) [23], carbon paste electrodes (CPEs) [24], metal nanoparticle-modified systems, and polymer-based electrodes. Despite their favorable conductivity and surface area, these platforms often require complex fabrication steps and may suffer from limited intrinsic catalytic activity, nanoparticle aggregation, or stability issues. Therefore, the development of carbon-based materials that combine high conductivity, abundant active sites, structural stability, and simple fabrication remains highly desirable.

ARTICLE IN PRESS

Compared with conventional carbon materials such as graphene and carbon nanotubes, Fe/N-doped graphene provides a higher density of active sites and improved charge-transfer efficiency [25,26]. Unlike metal oxide-based materials, which suffer from limited conductivity, the Fe/N-doped graphene system integrates high conductivity with a high density of accessible electroactive sites, resulting in enhanced sensor performance.

In this work, a Fe-containing N-doped graphene (Fe/N-Gr) hybrid nanostructure-modified GCE sensor (Fe/N-Gr/GCE) is developed as a green and sensitive electrochemical sensor for the detection and quantification of APRE in biological and pharmaceutical samples. Electrode fabrication and sensing conditions were optimized using CV and DPV, resulting in improved electrochemical response, enhanced interfacial electron-transfer kinetics, and a significantly increased electroactive surface area. The proposed sensor exhibited high stability and reproducibility, and was successfully applied to the determination of APRE in synthetic human serum, urine, and pharmaceutical tablet samples with high accuracy. By integrating a green synthesis strategy, rational electrode surface engineering, and sensitive electroanalytical techniques, this study demonstrates the potential of Fe/N-Gr-based electrochemical platforms as efficient, cost-effective, and environmentally friendly alternatives to conventional analytical methods for pharmaceutical and clinical analysis of apremilast.

ARTICLE IN PRESS

2. Experimental Approach

2.1. Materials and Reagents

All details related to the analytical instrumentation and operational parameters are reported in the Supplementary Material.

ARTICLE IN PRESS

2.2. Synthesis of Fe/N-Gr hybrid nanocomposite

Fe/N-Gr hybrid nanostructures were synthesized via a facile and environmentally benign aqueous hydrothermal route involving iron ion immobilization, nitrogen incorporation, and simultaneous reduction of graphene oxide (GO). GO was synthesized according to the modified Hummers' method [27-29] .

500 mg of GO was ultrasonically dispersed in 100 mL of deionized (DI) water (5.0 mg mL^{-1}) for 45 min to obtain a stable and homogeneous suspension. Subsequently, an aqueous solution of iron (III) chloride hexahydrate ($FeCl_3 \cdot 6H_2O$, 20 mM) was added dropwise to the GO dispersion under continuous magnetic stirring final Fe^{3+} concentration of 20 mM in the reaction mixture. The mixture was stirred for 3 h at room temperature to allow coordination and adsorption of Fe^{3+} species onto the oxygen-containing functional groups of GO sheets.

Subsequently, urea (1.0 g) was then introduced into the suspension as a nitrogen source, followed by the addition of L-ascorbic acid (200 mg) as a green reducing agent. The resulting mixture was stirred for an additional 15 min to ensure uniform distribution of the reagents. The suspension was subsequently transferred into a Teflon-lined stainless-steel autoclave, subjected to hydrothermal treatment at 180 °C for 12 h.

During the hydrothermal process, GO was reduced to graphene, nitrogen-containing functionalities were introduced into the graphene-based framework through urea decomposition, and Fe species were immobilized on the nitrogen-functionalized/doped graphene matrix. After the reaction, the autoclave was allowed to cool naturally to room temperature. The resulting black precipitate was collected by centrifugation at 8000 rpm

ARTICLE IN PRESS

for 10 min and washed repeatedly with DI water and ethanol until the supernatant became colorless, ensuring removal of residual ions and unreacted species. The final product was dried under vacuum at 60 °C for 12 h, yielding Fe/N-Gr as a fine black powder. The term Fe/N-Gr is therefore used to denote a Fe-containing nitrogen-functionalized/doped graphene hybrid structure, while the exact atomic-scale coordination environment of Fe is evaluated cautiously based on the available XRD, XPS, Raman, SEM, and TEM evidence.

The synthesis was carried out under fixed laboratory-scale conditions, including constant GO concentration, $FeCl_3$ concentration, urea amount, ascorbic acid amount, hydrothermal temperature, and reaction time. These controlled parameters were used to improve preparation consistency. However, direct quantitative batch-to-batch compositional analysis of Fe/N-Gr was not performed in the present study.

ARTICLE IN PRESS

2.3. Structural and Physicochemical Characterization

The structural, morphological, and surface chemical characteristics of the synthesized Fe/N-Gr nanosheets were investigated prior to electrode fabrication to verify graphene reduction, heteroatom incorporation, and successful modification with Fe species. The surface morphology and nanosheet structure of Fe/N-Gr were examined using scanning electron microscopy (SEM) (Quanta 650 FEG, FEI Company, Hillsboro, OR, USA). Transmission electron microscopy (TEM) was employed to further assess the nanoscale features, sheet morphology, and dispersion of Fe-containing domains on the graphene matrix.

ARTICLE IN PRESS

The crystallographic structure of the prepared materials was analyzed by X-ray diffraction (XRD) using an X'Pert PRO PANalytical diffractometer (Malvern Panalytical, Malvern, UK) with Cu Kα radiation (λ = 1.5406 Å), allowing evaluation of graphitic ordering and structural changes following reduction and modification.

Raman spectroscopy (Renishaw inVia Raman spectrometer) was conducted to investigate the graphitic structure, defect density, and disorder within the graphene framework. The relative intensities of the characteristic D and G bands were used to assess structural modifications induced by nitrogen incorporation and Fe interaction. Surface elemental composition and chemical bonding states were analyzed by X-ray photoelectron spectroscopy (XPS) using a Thermo Scientific K-Alpha instrument. High-resolution spectra of the C 1s, N 1s, O 1s, and Fe 2p regions were recorded and deconvoluted to identify the corresponding chemical states and confirm the presence of nitrogen functionalities and Fe species within the Fe/N-Gr architecture.

The combined characterization workflow was designed to verify the representative morphology, crystallographic structure, defect characteristics, surface elemental composition, and chemical states of the synthesized Fe/N-Gr nanostructure. While the representative material was structurally and chemically characterized by SEM, TEM, XRD, Raman spectroscopy, and XPS, direct quantitative batch-to-batch reproducibility of Fe loading, total nitrogen content, and large-scale scalability was not assessed in the present study. Future work may therefore include multi-batch synthesis combined with ICP-OES, CHN elemental analysis, and repeated structural characterization to establish compositional reproducibility and scalability.

2.4. Preparation of Fe/N-Gr/GCE Electrochemical Sensor

ARTICLE IN PRESS

A glassy carbon electrode (GCE, 3 mm diameter) was employed as the working electrode throughout the electrochemical experiments. Prior to surface modification, the GCE was polished on a microcloth pad using 0.3 μm alumina slurry for 5 min to obtain a smooth and reproducible surface. The electrode was then thoroughly rinsed with deionized water and subsequently sonicated in an ethanol-water mixture (1:1, v/v) for 5 min to remove residual alumina particles. After cleaning, the electrode was dried at room temperature.

For electrode modification, a dispersion of Fe/N-Gr was prepared by dispersing the nanocomposite in deionized water at a concentration of 1.0 mg mL^{-1}, followed by ultrasonication for 30 min to obtain a homogeneous suspension. An aliquot of 4.0 μL of the Fe/N-Gr dispersion was drop-cast onto the pretreated GCE surface and dried under infrared illumination for 10 min. The resulting Fe/N-Gr-modified GCE (Fe/N-Gr/GCE) was used directly for subsequent electrochemical characterization and analytical measurements.

ARTICLE IN PRESS

2.5. Electrochemical analysis

All electrochemical measurements were carried out using a conventional three-electrode system. An as-fabricated Fe/N-Gr/GCE electrode was used as the working electrode, a platinum wire served as the counter electrode, and an Ag/AgCl (3.0 M KCl) electrode was employed as the reference electrode. Electrochemical experiments were performed at room temperature (25 ± 2 °C) using an AUTO LAB system with PGSTAT204 electrochemical workstation (Metrohm Inc., Switzerland).

CV experiments were employed to investigate the electrochemical behavior, electron-transfer kinetics, and mass-transport characteristics of APRE, as well as to evaluate the

ARTICLE IN PRESS

interfacial properties of the modified electrode. Differential pulse voltammetry was used for quantitative analysis owing to its enhanced sensitivity and effective suppression of capacitive background currents.

DPV measurements were performed using a pulse amplitude of 50 mV, modulation time of 10 ms, step potential of 5 mV, and a scan rate of 50 mV s^{-1}. Electrochemical impedance spectroscopy (EIS) measurements were carried out in a solution containing 5.0 mM $[Fe(CN)_6]^{3-/4-}$ and 0.1 M KCl at an applied potential of 0.20 V over a frequency range of 1×10^5 to 0.1 Hz with an AC perturbation amplitude of 0.01 V. The impedance spectra were analyzed using a Randles equivalent circuit model comprising solution resistance (R_s), charge-transfer resistance (Rct), a constant phase element (CPE), and Warburg impedance (Zw). All electrochemical data were recorded at least in triplicate to ensure reproducibility, and the average values were used for quantitative analysis.

ARTICLE IN PRESS

2.6. Real Sample Preparation for Analysis

The practical applicability of the Fe/N-Gr/GCE was evaluated by determining APRE in real samples, including synthetic human serum, urine, and pharmaceutical tablet formulations. All real-sample analyses were carried out using the standard addition method to minimize potential matrix effects. Detailed sample preparation procedures for each matrix are provided in the S.M. file.

3. Results and discussion

3.1. Physicochemical Characterizations of Fe/N-Gr Nanostructure

The morphology and microstructural features of the synthesized Fe/N-Gr were investigated by SEM and TEM to elucidate the graphene framework and the distribution

ARTICLE IN PRESS

of Fe species. As shown in Figure 2A, the low-magnification SEM image reveals an interconnected, sheet-like morphology extending over large areas, indicative of a graphene-derived material rather than particulate carbon. The absence of dense agglomerates or spherical morphologies suggests that the material predominantly consists of stacked and intertwined nanosheets. At higher magnifications (Figure 2B-C), the SEM image clearly shows crumpled and wrinkled thin-sheet graphene texture with overlapping edges, a characteristic feature of reduced graphene oxide-based materials. Such corrugation and folding are commonly associated with the removal of oxygen-containing functional groups during reduction and with heteroatom incorporation, which disrupts planar stacking and suppresses restacking of graphene layers. TEM analysis (Figure 2D) provides additional insight into the nanoscale structure of Fe/N-Gr. The TEM image displays semi-transparent, thin graphene sheets with pronounced wrinkles and folds, confirming the exfoliated nature of the graphene framework. Several darker nanoscale contrast regions observed on the basal plane and along folded/edge regions of the sheets are attributed to Fe-associated domains with higher electron density than the carbon matrix. Importantly, these regions appear finely dispersed without the formation of large crystalline particles, supporting a microstructure in which Fe species are immobilized on the graphene surface in a dispersed form. However, since TEM contrast alone is not element-specific, this assignment is considered together with the complementary elemental and surface analyses. Importantly, no large crystalline Fe-based aggregates are observed, suggesting that Fe species are incorporated in a relatively dispersed form within the N-doped graphene architecture. Taken together, the SEM and TEM observations support the formation of interconnected graphene-derived

ARTICLE IN PRESS

nanosheets containing dispersed high-contrast Fe-associated domains, providing a favorable structural platform for enhanced interfacial electron transfer and electrochemical sensing performance.

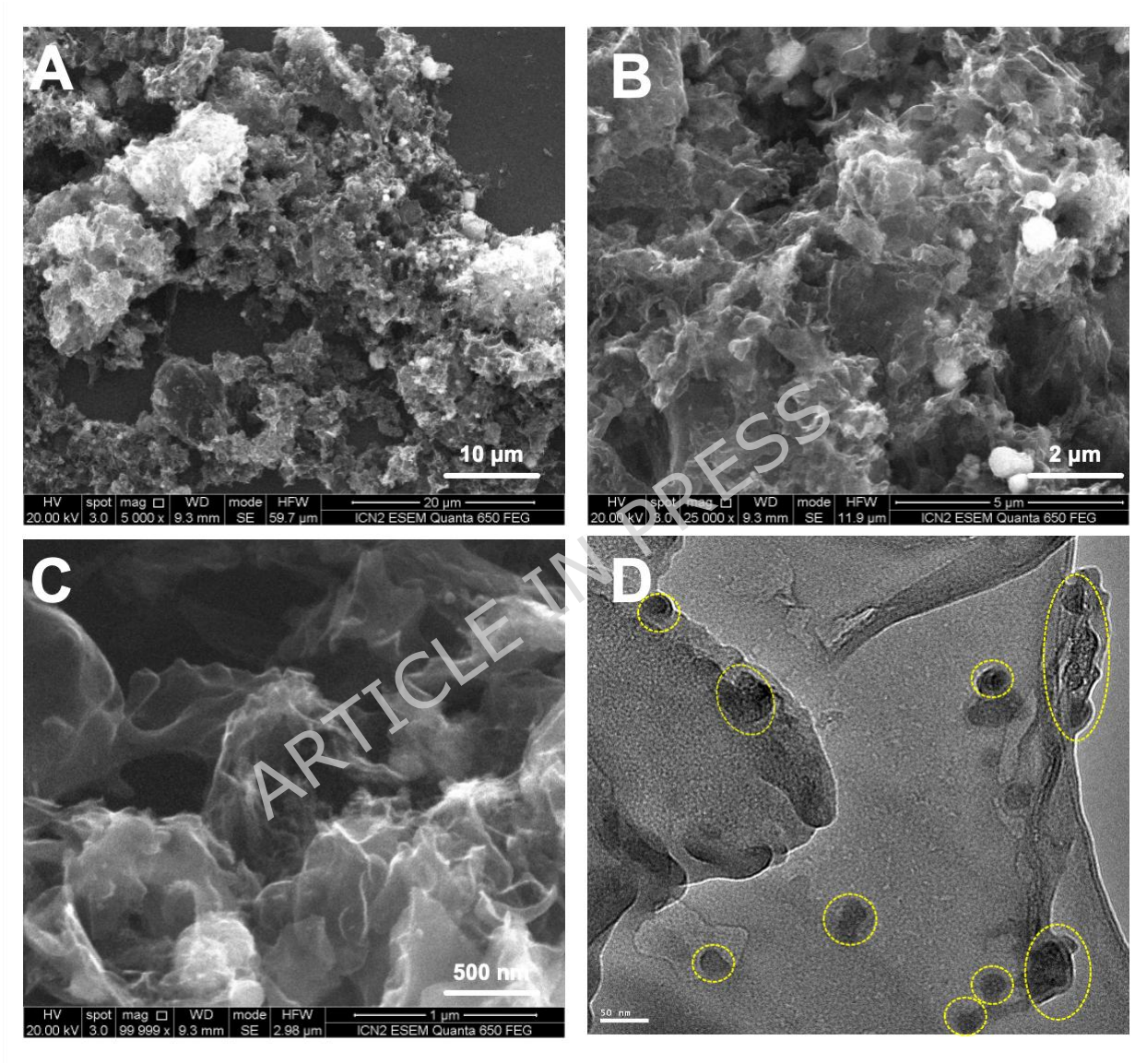


Figure 2. (A-C) SEM images of the hybrid nanostructure at different magnifications, showing the wrinkled and interconnected graphene-like morphology. (D) TEM image of Fe/N-containing graphene with representative Fe-associated nanodomains indicated by yellow dashed circles.

ARTICLE IN PRESS

The crystalline structure and phase composition of the synthesized Fe/N-Gr nanocomposite were investigated by XRD to elucidate the structural characteristics of the graphene framework and to identify the nature of the iron-containing phases (**Figure 3**). The XRD pattern is dominated by a broad diffraction feature centered at $2\theta \approx 26.7°$, which corresponds to the (002) reflection of graphitic carbon [30]. The pronounced broadening of this peak indicates a low degree of long-range stacking order along the c-axis, which is characteristic of few-layer, disordered graphene nanosheets derived from the reduction of graphene oxide. Using the Scherrer equation (see S.M file) [31-33] applied to the (002) reflection, the apparent coherent stacking thickness along the c-axis was estimated to be approximately 2.83 nm, with an interlayer spacing of ~0.334 nm. However, this value should be interpreted cautiously because peak broadening in reduced graphene oxide-derived and heteroatom-functionalized graphene materials is affected not only by finite stacking thickness, but also by turbostratic disorder, lattice defects, strain, and heterogeneous restacking. Therefore, the Scherrer-derived value is considered here as an approximate indicator of limited coherent stacking rather than a definitive measurement of crystallite size or exact layer number.

The few-layer and weakly stacked nature of Fe/N-Gr is therefore supported by the combined characterization results rather than by XRD alone. SEM and TEM observations reveal crumpled, wrinkled, and semi-transparent nanosheets with overlapping edges, while Raman spectroscopy shows a defect-rich sp^2 carbon framework with an ID/IG ratio of approximately 0.99 and a weak, broadened 2D-band feature. These complementary findings are consistent with a disordered few-layer graphene architecture with limited long-range stacking order. More direct determination of layer thickness would require

ARTICLE IN PRESS

additional techniques such as AFM height profiling, cross-sectional TEM, high-resolution TEM, or statistical thickness analysis.

In addition to the graphitic contribution, several weak but discernible diffraction peaks are observed at approximately 30.3°, 35.6°, 43.1°, 57.2°, and 62.8°. These reflections are in good agreement with standard crystallographic data for spinel-type iron oxide phases, particularly Fe_3O_4 (COD No. 9006189) [34] and γ-Fe_2O_3 (COD No. 9000139) [35] and can be indexed to the (220), (311), (400), (422), and (511) planes , respectively. These align with JCPDS/ICDD cards like 19-629 (Fe_3O_4) and 39-1346 (γ-Fe_2O_3) [36,37] . Because Fe_3O_4 and γ-Fe_2O_3 possess closely related spinel structures with highly overlapping XRD reflections, particularly in nanosized and weakly crystalline domains, the present XRD data do not allow definitive discrimination between these two phases. Therefore, the iron-containing component is described as dispersed spinel-type FeO_x domains, most likely Fe_3O_4 and/or γ-Fe_2O_3, rather than as a conclusively resolved dual-phase system. Moreover, the relatively low intensity and broad nature of these peaks suggest that the iron oxide domains are present in low concentration and/or with nanoscale crystallite dimensions, exhibiting limited long-range crystallinity. Notably, no characteristic diffraction peaks corresponding to metallic iron (Fe^0), iron carbide (Fe_3C), or wüstite (FeO) are detected, indicating that iron does not exist as bulk metallic or carbide phases. Instead, iron is present predominantly as dispersed spinel-type FeO_x domains associated with the graphene framework, as supported by the XRD peak positions, oxidized Fe^{2+}/Fe^{3+} features in the Fe 2p XPS spectrum, Fe-O contribution in the O 1s spectrum, and TEM contrast observations. Note that the dominance of the graphitic (002) reflection further confirms that the graphene framework constitutes the primary structural

ARTICLE IN PRESS

phase of the composite. From an electrochemical perspective, the combination of a defect-rich, few-layer graphene scaffold and weakly crystalline nanoscale iron oxide domains is advantageous, as it promotes efficient electron transport, enhances interfacial charge-transfer kinetics, and maximizes the accessibility of electroactive sites. Overall, the XRD analysis confirms the successful formation of a graphene-dominant Fe/N-Gr hybrid structure, composed of disordered few-layer graphene nanosheets and dispersed spinel iron oxide domains, providing a robust structural foundation for the enhanced electrochemical sensing performance observed.

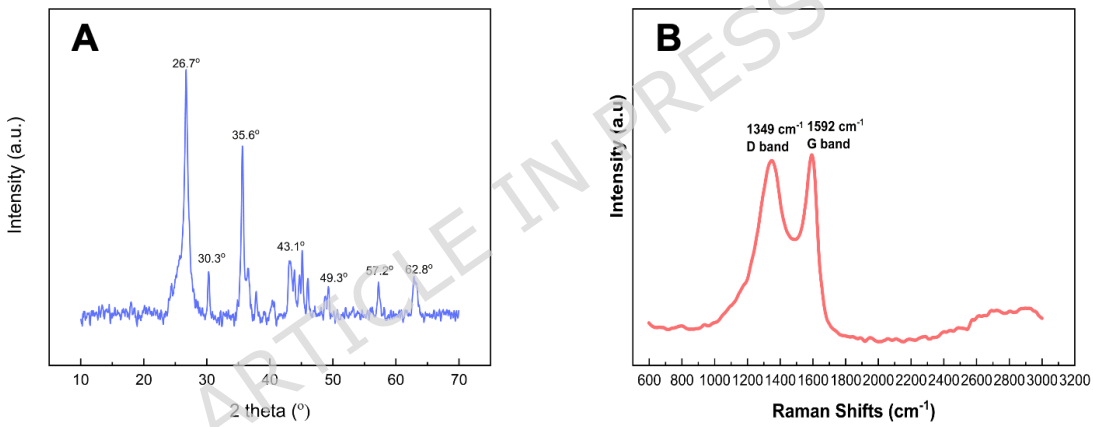


Figure 3. (A) XRD pattern (baseline-corrected) (B) Raman spectrum of Fe/N-Gr

Raman spectroscopy was employed to further evaluate the structural order and defect characteristics of the Fe/N-Gr nanocomposite. As shown in Figure 3B, the Raman spectrum exhibits two prominent bands centered at approximately 1349 cm^{-1} (D band) and 1592 cm^{-1} (G band), which are characteristic of graphene-based materials. The D band arises from defect-induced breathing modes of sp^2 carbon rings, while the G band corresponds to the in-plane vibrational mode of sp^2-hybridized carbon atoms within the

ARTICLE IN PRESS

graphene lattice. The intensity ratio of the D and G bands ($I_D/I_G \approx 0.99$) indicates a defect-rich sp^2 carbon network, which can be attributed to the reduction of graphene oxide, nitrogen functionalization/doping, including a graphitic-N contribution consistent with partial lattice incorporation, and the interaction of iron species with the graphene framework. Such structural disorder is commonly observed in heteroatom-doped graphene materials and is consistent with the disordered, few-layer structure. A weak and broadened feature in the 2D band region (~2700 cm^{-1}) is also observed, suggesting the presence of few-layer graphene with limited long-range stacking order rather than well-ordered multilayer graphite. This observation further corroborates the XRD results, which indicate a reduced stacking thickness and disordered graphene architecture.

XPS analysis was employed to investigate the surface elemental composition and chemical bonding states of Fe/N-Gr, as surface chemistry plays a critical role in governing electrochemical behavior and interfacial electron-transfer processes. The full-range XPS survey spectrum (**Figure 4A**) confirms the presence of C, O, N, and Fe, demonstrating the successful incorporation of nitrogen functionalities and iron species within the graphene-based architecture. The high-resolution C 1s spectrum of Fe/N-Gr exhibits (**Figure 4B**) a dominant peak centered at approximately 284.3 eV, which is attributed to sp^2-hybridized C=C bonds characteristic of the graphene lattice. Additional components observed at higher binding energies correspond to C=N, C-O, and C=O/O-C=O species. The presence of C-N bonds supports the successful introduction of nitrogen-containing functionalities into the graphene-based framework, although XPS alone cannot distinguish all surface-bound nitrogen species from substitutional lattice nitrogen with atomic-level certainty. These results confirm the formation of a conductive graphene

ARTICLE IN PRESS

scaffold with heteroatom-induced structural perturbations, which are beneficial for electrochemical applications. The N 1s spectrum (**Figure 4C**) reveals distinct contributions corresponding to different nitrogen bonding configurations within the graphene lattice. For the N 1s analysis, peak deconvolution was performed after background subtraction using chemically reasonable binding-energy windows for nitrogen-doped graphene materials. The fitted components were assigned based on commonly reported N 1s binding-energy ranges, while maintaining comparable peak-width constraints during fitting. Deconvolution of the N 1s region shows peaks typically assigned to pyridinic-N (~398.1 eV), pyrrolic-N (~399.8 eV), graphitic/quaternary-N (~400.8 eV), and N-oxide species (~403.3 eV). Pyridinic and pyrrolic nitrogen species are commonly associated with edge and defect sites, where they can act as active centers for adsorption and facilitate charge transfer. The graphitic/quaternary-N contribution is consistent with partial substitutional incorporation of nitrogen into the conjugated carbon framework and may contribute to improved electronic conductivity. However, the coexistence of these components should be interpreted as evidence of nitrogen functionalization/doping rather than as conclusive proof of exclusive lattice incorporation. Thus, the XPS results support the formation of a defect-rich nitrogen-functionalized graphene surface containing both lattice-associated and edge/defect-associated nitrogen species. Moreover, since the present study does not establish a quantitative species-resolved correlation between individual nitrogen configurations and the APRE oxidation current, the enhanced electrochemical response is attributed to the collective contribution of nitrogen functionalization/doping, defect-rich graphene structure, increased

ARTICLE IN PRESS

electroactive surface area, and dispersed oxidized Fe species, rather than to a single nitrogen species.

The O 1s high-resolution spectrum **(Figure 4D**) provides further insight into the oxygen functionalities present in Fe/N-Gr. The fitted profile consists of multiple components that can be ascribed to oxygen-containing functional groups on the graphene surface and oxygen bound to iron. The lower binding-energy contribution (around ~529-531 eV) is consistent with metal-oxygen (Fe-O) and C=O bonding, supporting the presence of oxidized Fe species strongly associated with the carbon matrix. The dominant component centered in the ~531-533 eV region can be assigned to C-O-type species (e.g., hydroxyl/ether functionalities), while the higher binding-energy contribution (~533-536 eV) corresponds to more oxidized oxygen environments such as O-C=O groups. The coexistence of Fe-O and C-O/C=O-related components indicates that the graphene framework is reduced yet retains a controlled amount of surface oxygen functionality. These residual oxygen groups are beneficial because they can act as anchoring sites that stabilize Fe species on the graphene surface, limit particle growth/aggregation, and promote intimate interfacial contact, thereby supporting efficient charge transfer in electrochemical operation.

The Fe 2p spectrum (**Figure 4E**) displays characteristic Fe $2p_3/_2$ and Fe $2p_1/_2$ peaks located at approximately 710-712 eV and 724-726 eV, respectively, accompanied by satellite features. The Fe 2p spectrum exhibits features consistent with oxidized iron species, including contributions that can be assigned to Fe^{2+}/Fe^{3+}-type environments and accompanying satellite structures. Importantly, these data do not provide definitive evidence for atomically dispersed Fe-N_x coordination as the dominant Fe environment.

ARTICLE IN PRESS

Instead, when considered together with the weak XRD reflections assigned to spinel-type iron oxide phases and the Fe-O contribution observed in the O 1s spectrum, the Fe 2p results indicate that Fe is predominantly present as dispersed oxidized FeO_x-type domains associated with the nitrogen-functionalized graphene matrix. Nevertheless, due to the strong overlap between Fe_3O_4 and γ-Fe_2O_3 signatures in conventional XRD and Fe 2p XPS, the present data should be interpreted as evidence for dispersed spinel-type FeOx species rather than definitive proof of a resolved Fe_3O_4/γ-Fe_2O_3 dual phase. The absence of metallic Fe^0 features in the Fe 2p spectrum further confirms that iron is present predominantly in an oxidized form rather than as metallic nanoparticles. The presence of oxidized Fe species may be beneficial for electrochemical sensing because FeOx domains can facilitate interfacial charge transfer and contribute to the electrochemical activity of the modified electrode. These findings are in good agreement with the XRD results, which reveal weak diffraction peaks attributed to nanoscale iron oxide domains, and with TEM observations showing dispersed Fe-containing contrast regions.

The XPS results support the successful formation of Fe-containing nitrogen-functionalized/doped graphene nanosheets composed of a conductive graphene backbone enriched with heteroatom-induced defect sites and associated with finely dispersed mixed-valence FeOx species. This synergistic surface chemistry is expected to promote efficient electron transfer, enhance analyte adsorption, and amplify electrochemical signals, thereby underpinning the superior analytical performance of the Fe/N-Gr-modified electrode for APRE detection.

It should also be noted that the present XRD, XPS, Raman, SEM, and TEM results are sufficient to support nitrogen functionalization/doping and FeOx immobilization, but they

ARTICLE IN PRESS

do not allow an unambiguous atomic-scale assignment of Fe coordination. Definitive discrimination between Fe-N_x sites and FeO_x coordination environments would require local-structure-sensitive techniques such as Fe K-edge XANES/EXAFS, Mössbauer spectroscopy, or atomic-resolution STEM-EELS. Therefore, the enhanced electrochemical performance observed in this work is attributed to the combined effects of the conductive nitrogen-functionalized graphene framework, defect/edge-associated nitrogen sites, and dispersed mixed-valence FeOx domains rather than to a specifically assigned Fe-N_x structure.

ARTICLE IN PRESS

ARTICLE IN PRESS

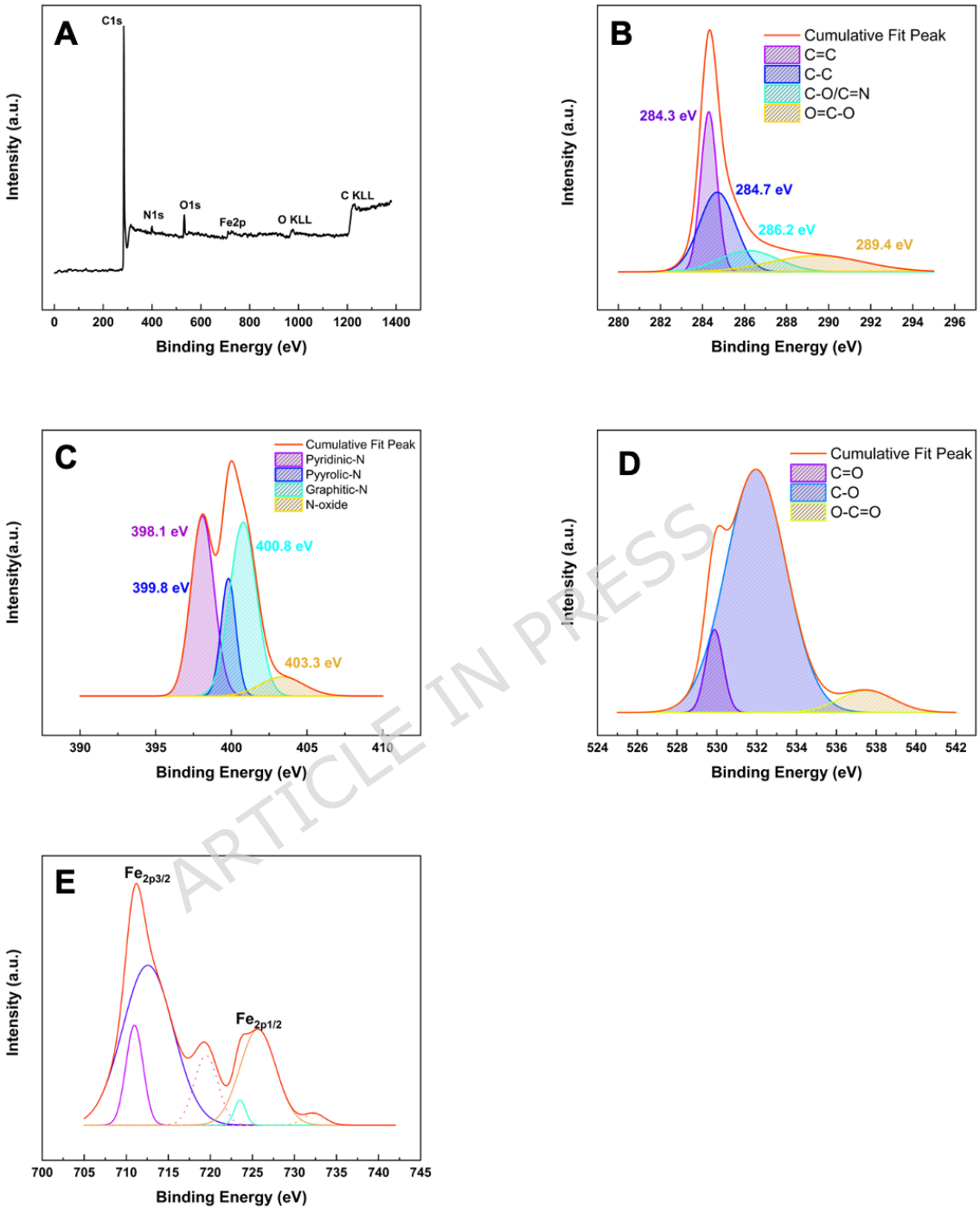


Figure 4. XPS characterization of Fe/N-Gr (A) Survey spectrum; (B) C 1s; (C) N 1s; (D) O 1s; (E) Fe 2p high-resolution spectra

ARTICLE IN PRESS

3.2. Electrochemical Behavior of Fe/N-Gr/GCE

The interfacial electron-transfer characteristics of the bare GCE and the Fe/N-Gr/GCE were comparatively evaluated by CV and EIS using the reversible redox probe $[Fe(CN)_6]^{3-/4-}$ (5.0 mM) in 0.1 M KCl. As depicted in Figure 5A, both electrodes exhibited well-defined and reversible redox peaks, indicating effective electrochemical activity. Furthermore, modification with the Fe/N-Gr nanocomposite resulted in a pronounced enhancement of the redox peak currents together with a substantial reduction in the peak-to-peak potential separation. Specifically, the anodic peak current increased from 3.50×10^{-5} A at the bare GCE to 4.55×10^{-5} A at the modified electrode, while ΔE_p decreased from 142 to 102 mV. These observations clearly indicate improved interfacial charge-transfer kinetics, which can be attributed to the increased electroactive surface area and enhanced electrical conductivity imparted by the Fe/N-Gr nanocomposite layer.

To further elucidate the charge-transfer mechanism, CV was conducted at scan rates ranging from 25 to 225 mV s^{-1} (Figure S1). The anodic peak current exhibited a proportional dependence on the square root of the scan rate, confirming that the electrooxidation process is governed primarily by diffusion. The electroactive surface area (ESA), calculated using the Randles-Ševčík equation [38], increased from 0.07 cm^2 for the unmodified GCE to 0.14 cm^2 after modification with the Fe/N-Gr nanocomposite. This notable increase demonstrates that the surface engineering strategy effectively enlarges the accessible active area and facilitates more efficient interfacial charge transport, thereby enhancing the overall electrochemical performance of the sensing platform.

ARTICLE IN PRESS

The interfacial electrochemical properties of the unmodified and Fe/N-Gr-functionalized GCE were systematically investigated by EIS under ambient conditions. Nyquist spectra were recorded in a solution containing 5.0 mM $[Fe(CN)_6]^{3-/4-}$ and 0.1 M KCl at an applied potential of 0.2 V (Figure 5B). The EIS data were fitted to the corresponding Randles equivalent circuit, as illustrated in Figure 5B. The quality of the fitting was evaluated using the chi-square (χ^2) parameter, yielding values of 0.124 for the bare GCE and 0.035 for the Fe/N-Gr-modified GCE, confirming excellent agreement between the experimental data and the fitted model. For both electrodes, the impedance profiles display a depressed semicircle in the high-frequency area, corresponding to the charge-transfer process, followed by a linear region at lower frequencies associated with diffusion-controlled mass transport. Moreover, surface modification with the Fe/N-Gr nanocomposite results in a substantial decrease in the semicircle diameter, reflecting a marked decrease in charge-transfer resistance. However, the Rct value decreases from 3.9 kΩ for the bare GCE to 1.7 kΩ for the modified electrode, evidencing enhanced interfacial conductivity and more efficient electron-transfer kinetics. These results clearly demonstrate that the incorporation of Fe/N-Gr nanocomposite facilitates rapid charge transport at the electrode-electrolyte interface, thereby improving the overall electrochemical performance of the sensing platform.

This behavior can be attributed to the synergistic contribution of the conductive Fe/N-Gr framework, the increased electroactive surface area, and the accessible electroactive sites, which facilitate enhanced charge transport at the electrode-electrolyte interface. Consequently, these characteristics lead to improved interfacial electron-transfer kinetics and overall electrochemical performance of the proposed sensing platform.

ARTICLE IN PRESS

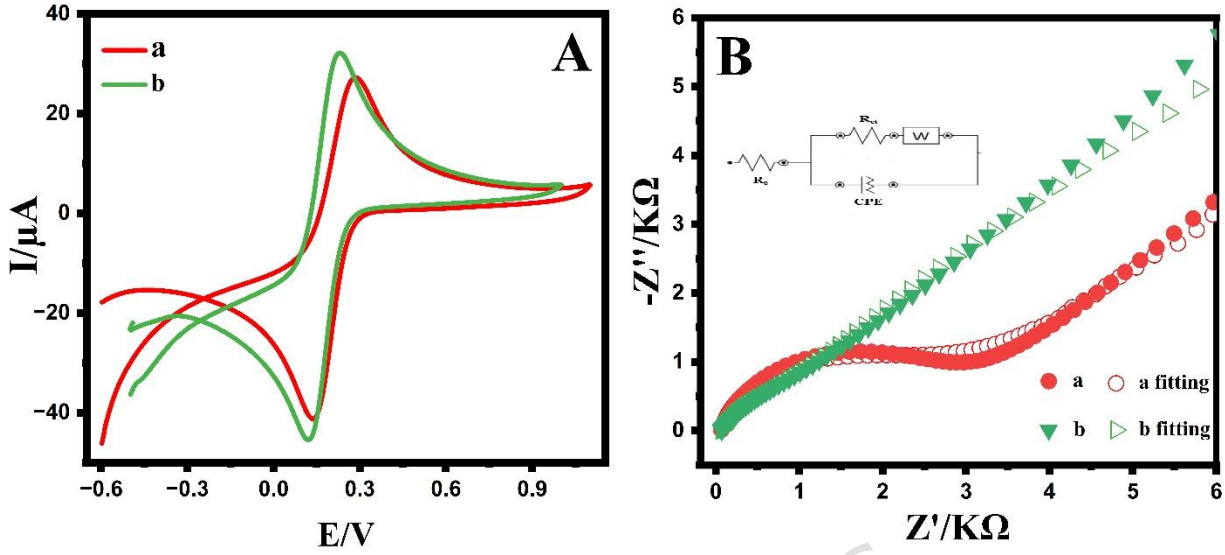


Figure 5. (A) CVs and (B) EIS of the unmodified GCE (a) and Fe/N-Gr/GCE (b) obtained in $[Fe(CN)_6]^{3-/4-}$ (5.0 mM).

3.3. Voltammetric Studies of APRE Using an Fe/N-Gr -Modified Electrode

The electrochemical response of APRE was systematically investigated at bare and Fe/N-Gr-functionalized GCE using CV and DPV, as depicted in Figure 6. Therefore, measurements conducted in a pH 2.0 BR solution in the absence of APRE resulted in only baseline currents for both electrodes, indicating that the supporting electrolyte does not contribute detectable redox processes within the examined potential window.

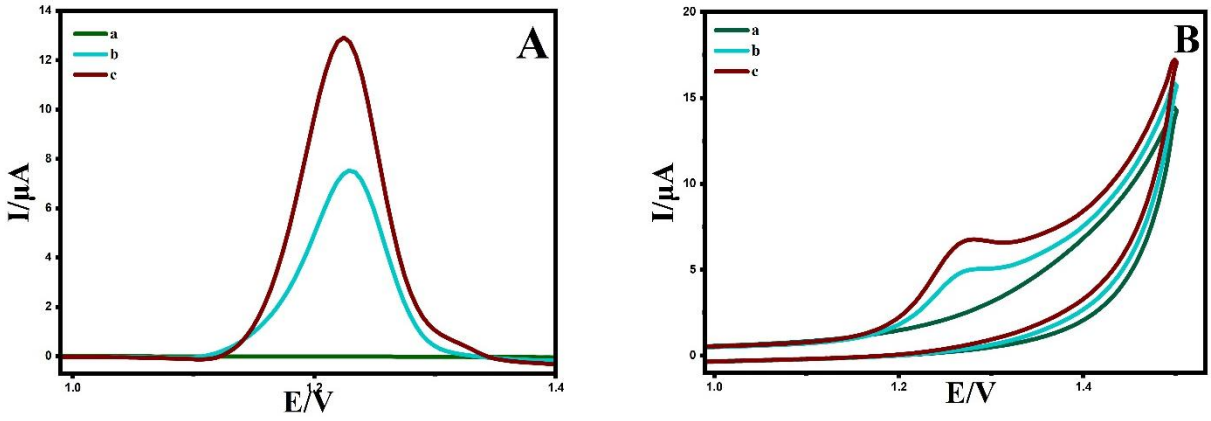
Upon the addition of 10 μM APRE, the unmodified GCE exhibited a weak anodic response with a peak current of 8.47×10^{-6} A and a peak potential of 1.24 V, indicating limited electron-transfer kinetics at the bare electrode surface. In contrast, the Fe/N-Gr-modified electrode showed a significantly higher oxidation current of 1.32×10^{-5} A with the peak potential shifted to 1.22 V. This decrease in peak potential indicates a lower oxidation

ARTICLE IN PRESS

overpotential at the modified interface. The observed differences in current response and peak position confirm enhanced charge-transfer behavior at the Fe/N-Gr-modified electrode, which can be attributed to the conductive network and the increased availability of electroactive sites provided by the nanocomposite.

Further evidence was obtained from CV measurements, which indicated that the electrooxidation of APRE proceeds via an irreversible process. The bare GCE exhibited an anodic peak current of 1.05×10^{-6} A at 1.27 V, whereas the Fe/N-Gr-modified electrode showed a higher peak current of 2.29×10^{-6} A at 1.266 V. The observed increase in current together with the slight shift in peak potential reflects changes in the electron-transfer process at the modified electrode surface. DPV measurements further enhanced analytical performance by yielding well-resolved oxidation peaks with suppressed background contributions, thereby enabling higher sensitivity and improved peak separation. Moreover, surface modification of the GCE with Fe/N-Gr significantly optimizes its electrochemical properties, establishing an effective and reliable sensing interface for the sensitive determination of APRE.

ARTICLE IN PRESS



ARTICLE IN PRESS

Figure 6. DPV and (B) CV 50.0 mV/s (B) of 10 μM APRE in 0.1 M BR solution at blank (a), bare GCE (b), and Fe/N-Gr/GCE (c).

3.4. Experimental Condition Optimization

3.4.1. Optimization of Experimental Parameters for the Sensor

The amount of Fe/N-Gr nanocomposite incorporated onto the electrode surface was optimized by monitoring its effect on the oxidation signal of APRE over a modifier concentration range of 0.1-2.0 mg·mL^{-1} (Figure S2A). The anodic peak current increased steadily with increasing nanocomposite concentration and reached its maximum at 1.0 mg·mL^{-1}, indicating more efficient interfacial charge transfer and greater exposure of electroactive sites. When the concentration exceeded this value, a decline in current response was observed, which is attributed to excessive surface coverage leading to increased film thickness and restricted mass transport of APRE toward the electrode interface. These observations demonstrate that excessive modifier loading can be detrimental to electrochemical performance, and thus 1.0 mg·mL^{-1} was selected as the optimal concentration for electrode modification.

The effect of modifier deposition volume on the electrochemical response of APRE was also examined by varying the applied volume of the Fe/N-Gr suspension from 4.0 to 8.0 μL in 0.1 M BR solution at pH 2.0 (Figure S2B). An increase in peak current was observed with increasing volume, reaching a maximum at 4.0 μL, which can be attributed to the formation of an electrochemically active and well-distributed modifier layer. Further increases in deposition volume resulted in diminished current responses, likely due to particle aggregation and the development of diffusion barriers that hinder effective

ARTICLE IN PRESS

electron transfer. Accordingly, deposition of 4.0 μL of a 1.0 mg·mL^{-1} Fe/N-Gr suspension was identified as the optimal configuration for achieving maximum electrochemical sensitivity.

3.4.2. Optimization of buffer composition and pH

The effect of the supporting electrolyte on the electrochemical oxidation response of APRE was systematically investigated using DPV. Several electrolyte systems, including phosphate-buffered saline (PBS), Britton-Robinson (BR) solution, potassium chloride (KCl), and hydrochloric acid (HCl), were evaluated to identify the most suitable medium for electroanalytical measurements. As illustrated in Figure S3A, the highest and most clearly defined oxidation peak for APRE was obtained in the BR solution. The enhanced response observed in the BR solution can be ascribed to its broad buffering capability and effective regulation of proton activity, which favors proton-assisted electron-transfer processes at the electrode surface and facilitates efficient charge transport across the electrode-solution interface. These properties result in improved peak sharpness, increased current intensity, and stable electrochemical behavior. Furthermore, the use of BR solution ensures consistent ionic strength and sustained proton availability, both of which are essential for achieving reproducible and reliable voltammetric responses. These findings demonstrate that the electrochemical performance of APRE is dependent on the composition of the electrolyte and the solution environment. Owing to the highest observed oxidation peak current (14 μA), together with a well-defined response and stable baseline, the BR buffer was selected as the optimal supporting electrolyte for all subsequent electrochemical studies.

ARTICLE IN PRESS

The influence of solution pH on the electrochemical response of APRE at the Fe/N-Gr/GCE was systematically assessed to establish optimal sensing conditions (Figure S3 B). DPV experiments were carried out in 0.1 M BR solution containing 10 μM APRE across a pH range of 2.0-8.0.

A pronounced dependence of peak current on electrolyte acidity was observed, with the highest anodic response occurring at pH 2.0, indicating that mildly acidic conditions favor enhanced interfacial electron-transfer efficiency and signal amplification.

The acidic conditions promote higher current responses, likely due to improved charge transport and surface interaction dynamics. Consequently, pH 2.0 was selected as the optimal working condition for all subsequent electroanalytical studies.

As can be seen in Figure S3 B, the negligible shift in anodic peak potential (E_{pa}) with pH indicates that the electrochemical oxidation of APRE is not significantly influenced by proton activity. This suggests that proton transfer is unlikely to be involved in the rate-determining step under the investigated experimental conditions. The observed behavior implies that the oxidation process is primarily governed by an electron-transfer mechanism, in which the number of transferred electrons remains constant over the studied pH range. Therefore, the electrochemical response is controlled by the intrinsic redox properties of APRE rather than proton-coupled processes in the solution.

ARTICLE IN PRESS

3.4.3. Impact of scan rate

The effect of scan rate on the electrochemical oxidation of APRE was studied in 0.1 M BR solution at pH 2.0, using scan rates from 25 to 300 $mV \cdot s^{-1}$. As shown in Figure 7A, the anodic peak current increased with increasing scan rate, and the oxidation peak

ARTICLE IN PRESS

shifted slightly toward more positive potentials. This behavior indicates an irreversible oxidation process controlled by electron-transfer kinetics. The absence of a cathodic peak during the reverse scan further confirms the irreversible nature of APRE oxidation under the applied conditions.

A linear relationship was obtained between the anodic peak current (I_p) and the square root of the scan rate ($v^{1/2}$), described by the equation $I_p = 0.226\ v^{1/2} + 0.414$ ($R^2 = 0.999$), as shown in Figure 7B. This linearity indicates that the oxidation of APRE is mainly controlled by diffusion of APRE molecules from the bulk solution to the electrode surface.

In addition, the plot of log I_{pa} versus log v (Figure 7C) showed a linear relationship with a slope of 0.528, which is close to the theoretical value of 0.5 expected for diffusion-controlled processes.

The dependence of the anodic peak potential (E_{pa}) on the natural logarithm of scan rate (ln v) was further analyzed using Laviron's model for irreversible electrochemical reactions (Figure 7D). According to Laviron's theory (Eq.1), the relationship between peak potential and scan rate for an irreversible electrochemical system can be expressed as follows:

$$E_{pa} = E^{\circ} + \left(\frac{RT}{\alpha nF}\right)\ln\left(\frac{RTK^{\circ}}{\alpha nF}\right) + \left(\frac{RT}{\alpha nF}\right)\ln v \qquad (1)$$

where K^{o} is the heterogeneous electron transfer rate constant, n is the number of electrons transferred, α is the charge transfer coefficient, v is the scan rate, T = 298 K, R = 8.314 J K^{-1} mol^{-1}, F = 96,480 C mol^{-1}, and E^0 is the formal redox potential.

ARTICLE IN PRESS

Using the slope of the E_{pa} versus ln v plot and Laviron's theory for irreversible electrochemical systems, the number of electrons involved in APRE oxidation was calculated as n = 2. To further investigate the electron-transfer kinetics of APRE oxidation, Tafel analysis was performed using the low-overpotential rising portion of the anodic branch of the cyclic voltammogram prior to the peak potential, where charge-transfer kinetics dominate (Figure S4). According to the Butler-Volmer relationship, the Tafel slope (0.164 V dec^{-1}), expressed as $2.3RT/n(1-\alpha)F$, was used to calculate the electron-transfer coefficient (α), which was determined to be approximately 0.82. This value indicates an asymmetric activation energy barrier for the irreversible electro-oxidation of APRE and is consistent with the irreversible behavior observed in the cyclic voltammograms. The Tafel analysis provides complementary kinetic information to the Laviron and EIS analyses. Together with the reduced charge-transfer resistance (Rct), increased heterogeneous electron-transfer rate constant (k_0), and smaller peak-to-peak potential separation (ΔEp) observed for the Fe/N-Gr/GCE, these results collectively demonstrate improved interfacial electron-transfer kinetics after electrode modification. These findings provide additional kinetic evidence supporting the enhanced electrochemical performance of the proposed sensing platform. These results support the proposed oxidation mechanism shown in Scheme 1.

ARTICLE IN PRESS

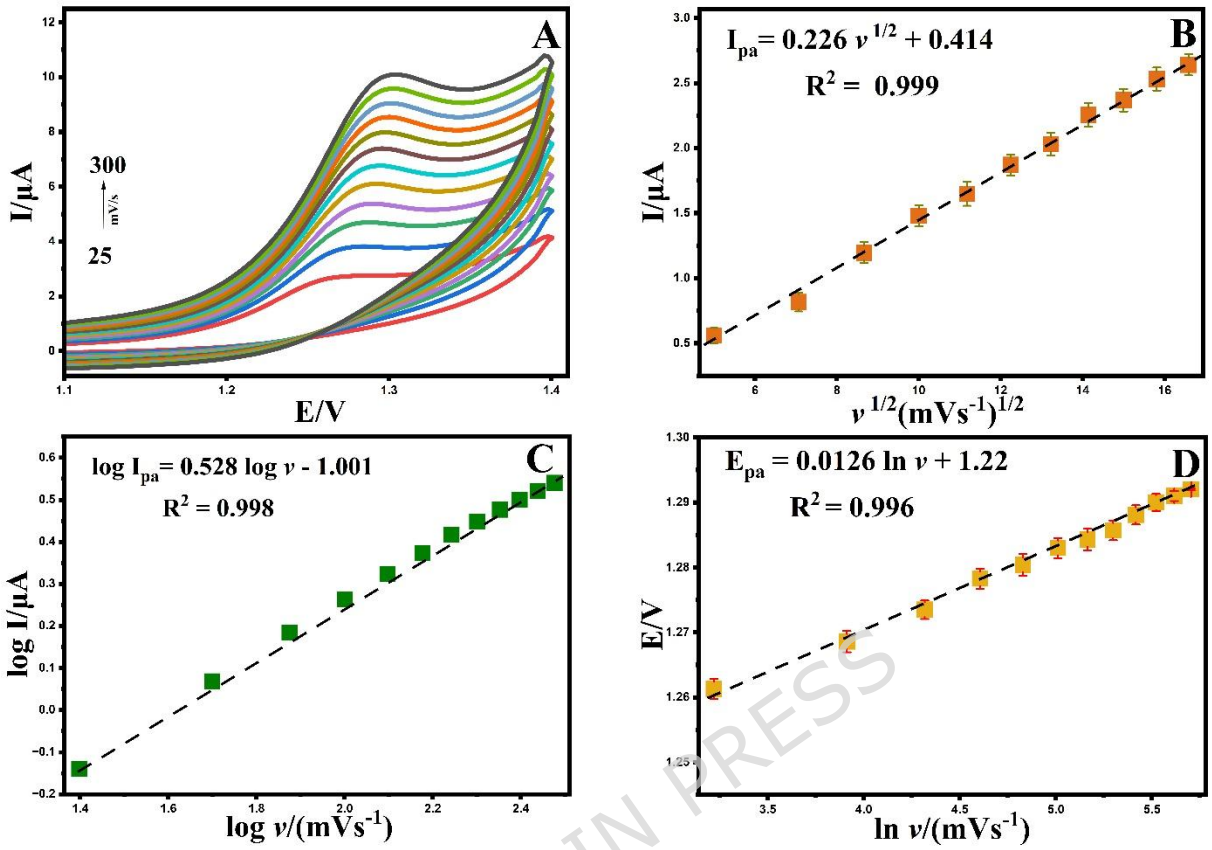
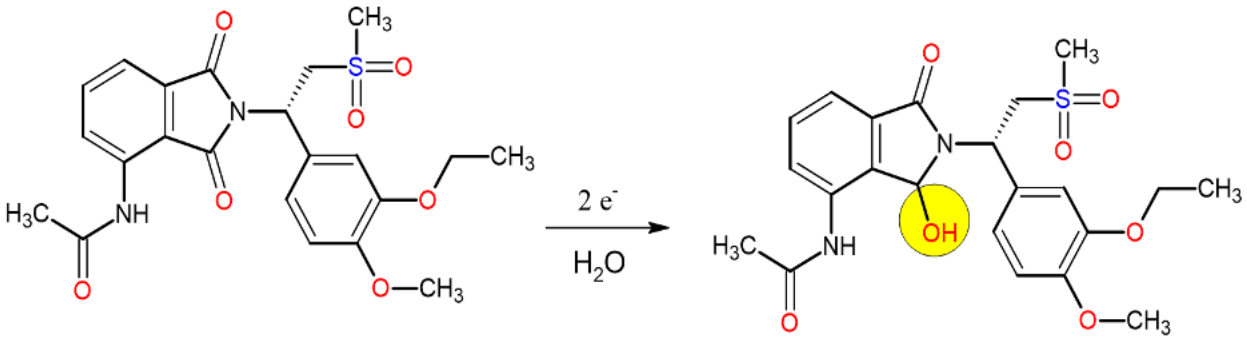


Figure 7. (A) Cyclic voltammograms of Fe/N-Gr/GCE recorded in 10 μM APRE prepared in BR solution (pH 2.0) at various scan rates; (B) plot of Ipa versus $v^{1/2}$; (C) plot of log Ipa against log v; and (D) plot of Epa versus ln v.



Scheme 1. illustrative mechanism depicting the electrochemical conversion of APRE

ARTICLE IN PRESS

3.5 Quantitative Analysis of APRE Using DPV

The electroanalytical performance of the Fe/N-Gr/GCE sensor was evaluated using DPV, with increasing concentrations of APRE in BR solution (pH 2.0), as illustrated in Figure 8. The anodic peak current (I_{pa}) increased linearly with APRE concentration over the range of 0.1-22.0 μM, yielding a correlation coefficient of $R^2 = 0.998$. Although a slight visual displacement of the oxidation peak can be observed in the overlaid DPV curves, the measured peak potential varied only within a narrow range across the investigated APRE concentrations. This minor variation is attributed to interfacial and experimental factors rather than to a change in the APRE oxidation mechanism. Importantly, the peak current increased linearly with APRE concentration, confirming the suitability of the Fe/N-Gr/GCE sensor for quantitative APRE determination. The resulting calibration equation was expressed as I_{pa} (μA) = 0.058 [APRE] + 0.021. The limit of detection (LOD) and limit of quantification (LOQ) were calculated according to the expressions $LOD = 3.3\sigma/S$ and $LOQ = 10\sigma/S$, where σ represents the standard deviation of the blank signal, and S is the slope of the calibration curve. Based on these calculations, the LOD and LOQ were determined to be 0.008 μM and 0.029 μM, respectively. These results demonstrate the high sensitivity, analytical reliability, and suitability of the Fe/N-Gr/GCE sensor for trace-level determination of APRE.

ARTICLE IN PRESS

ARTICLE IN PRESS

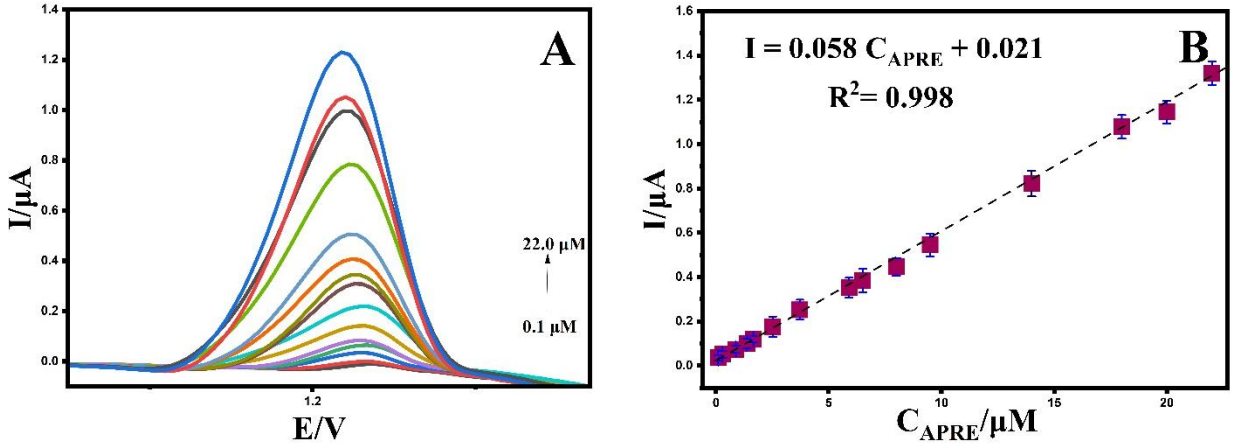


Figure 8. (A) DPV curves of varying concentrations of APRE on the Fe/N-Gr/GCE in BR solution (0.1 M, pH = 2.0) and (B) calibration plot of Ipa (μA) versus [APRE]/μM.

As shown in Table 1, the proposed electrochemical method is compared with previously reported analytical techniques for APRE determination. RP-HPLC and UPLC-MS/MS methods are based on chromatographic techniques and have been applied to tablet formulations and biological samples, respectively, while UV spectrophotometry has been used for pharmaceutical tablet analysis. In comparison, the developed Fe/N-Gr/GCE electrochemical sensor has been applied to human serum, urine, and pharmaceutical tablet samples. Regarding analytical performance, the proposed method shows competitive performance in terms of LOQ compared with some of the previously reported approaches. Overall, the developed sensor offers a reliable electrochemical alternative for APRE determination across different sample matrices.

Table 1. Comparison of the proposed electrochemical method with previously reported analytical methods for the determination of APRE.

Method	Linear Range	LOQ	Application	Ref

ARTICLE IN PRESS

RP-HPLC	2-12 µg/mL	0.416 µg/mL	Tablet formulation	[8]
UPLC-MS-MS	0.1-100 µg/mL	0.1 µg/mL	Rat plasma	[2]
UV spectrophotometric	2 -10 µg/mL	0.00271 µg/mL	Pharmaceutical tablet	[39]
Electrochemical (Fe/N-Gr/GCE sensor)	*0.1-22.0 µM*	*0.029 µM*	*Human serum, urine, and pharmaceutical tablet*	*Our work*

3.6. Anti-interference ability of Fe/N-Gr/GCE

Demonstrating high selectivity, the Fe/N-Gr sensor maintained a consistent and well-defined electrochemical response toward 1.0 µM APRE in the presence of coexisting species. The interference tolerance of the sensor was systematically evaluated by DPV using a variety of potential interferents commonly present in biological and pharmaceutical matrices, including ascorbic acid (A-A), uric acid (U-A), dopamine (DOP), L-arginine (L-A), L-methionine (L-M), paracetamol (PARA), caffeine (CAF), potassium chloride (KCL), potassium nitrate (KNO_3), and sodium sulfate (NA_2SO_4). In addition, the structurally related pharmaceutical compound lenalidomide was investigated to further assess the sensor's selectivity toward APRE. Each interfering substance was examined at concentrations up to 100-fold higher than that of APRE to simulate competitive conditions. As illustrated in Figure S5 and Table 2, the anodic peak current of APRE showed negligible variation in the presence of these species, with a relative standard deviation value of 1.81%, confirming stable signal response and reproducible

ARTICLE IN PRESS

electrochemical behavior. The observed selectivity can be attributed to the favorable interfacial characteristics of the Fe/N-Gr nanocomposite, which enhance electron-transfer efficiency for APRE while suppressing responses from competing electroactive species. These results confirm the strong anti-interference capability of the proposed sensor for reliable APRE detection.

Table 2. Selectivity of Fe/N-Gr-modified GCE for APRE in the presence of various compounds.

Interferent	**APRE: interferent**	**Oxidation current (μA)**	**Oxidation current change (%)**
Apremilast	**-----**	**0.103**	**------**
potassium chloride	1:100	0.10	-3.43
sodium nitrate	1:100	0.103	-0.59
sodium sulfate	1:100	0.102	-1.56
L-arginine,	1:100	0.102	-1.23
L-methionine	1:100	0.10	-3.02
ascorbic acid	1:100	0.103	-0.48
Caffein	1:100	0.105	+1.71
dopamine	1:100	0.10	-2.97
Paracetamol	1:100	0.102	-1.35
uric acid	1:100	0.10	-2.83
Lenalidomide	1:100	0.106	+2.05

ARTICLE IN PRESS

3.7. Evaluation of repeatability and reproducibility of the Fe/N-Gr/GCE sensor

The repeatability of the Fe/N-Gr/GCE sensor was assessed through eleven consecutive DPV measurements of 1.0 μM APRE using a single modified electrode under identical conditions (Figure S6). The resulting relative standard deviation (RSD) of 2.4% indicates

ARTICLE IN PRESS

consistent current responses, reflecting promising short-term precision. These findings confirm that the electrode surface maintains stable electron-transfer kinetics and is resilient to repeated measurements. The negligible variation in peak currents further demonstrates the robustness of the Fe/N-Gr nanocomposite in preserving electroactive sites, ensuring reliable and reproducible sensor performance for routine quantitative analysis.

The reproducibility of the Fe/N-Gr/GCE sensor was evaluated using eight independently fabricated electrodes prepared under identical conditions. The electrodes displayed consistent voltammetric responses, yielding a low RSD of 2.1% (Figure S7). This low variability indicates uniform surface modification and electrode morphology, along with consistent inter-electrode performance. Such results demonstrate the robustness of the fabrication protocol and confirm the suitability of the sensor for reproducible and reliable electroanalytical applications. It should be noted that this reproducibility assessment refers to the preparation and analytical response of independently modified electrodes. It does not represent direct quantitative batch-to-batch compositional validation of the Fe/N-Gr powder. Confirmation of nanomaterial-level reproducibility would require independent Fe/N-Gr synthesis batches followed by quantitative Fe loading analysis, total nitrogen determination, and repeated structural characterization. This point has been added as a limitation of the present study.

ARTICLE IN PRESS

3.8. Practical applicability of the Fe/N-Gr/GCE sensor to real-world samples

The practical applicability, analytical accuracy, and robustness of the Fe/N-Gr/GCE sensor were validated through real-sample analysis using DPV combined with the

ARTICLE IN PRESS

standard addition approach to effectively minimize matrix effects. The sensor was applied to the determination of APRE in synthetic human serum, urine, and pharmaceutical tablet samples. Known concentrations of APRE were spiked into each matrix within the established linear range, and recovery studies were conducted to evaluate analytical accuracy. As presented in Table 3, the recoveries ranged from 97.41% to 102.71%, with RSDs of 1.25-2.36%, indicating high precision and reproducibility. These RSD values suggest only minor matrix-induced variations, which are expected in complex biological media containing proteins, salts, and other electroactive species.

These results confirm that the Fe/N-Gr/GCE sensor maintains reliable analytical performance in complex matrices, characterized by strong selectivity, negligible interference, and stable signal responses. Moreover, the findings highlight the robustness and structural stability of the modified electrode, demonstrating its suitability as a dependable electroanalytical platform for the accurate and reproducible quantification of APRE in pharmaceutical formulations and biological samples under practical conditions.

ARTICLE IN PRESS

ARTICLE IN PRESS

Table 3. Determination of APRE in spiked samples

Sample	Added (μM)	Detected (μM)	RSD (%)	Recovery (%)
Synthetic Human serum	2.0	2.015	2.04	102.54
	4.0	3.966	1.74	99.18
	6.0	5.974	1.25	99.57
Synthetic Human urine	2.0	2.012	2.36	100.62
	4.0	3.951	2.31	97.86
	6.0	6.016	1.65	102.71
Pharmaceutical Tablet	2.0	2.005	1.61	100.29
	4.0	3.941	2.22	97.41
	6.0	5.954	1.25	99.08

ARTICLE IN PRESS

3.9. Green and Blue Chemistry Evaluation of the Developed Method

The environmental sustainability of the developed electrochemical strategy was systematically evaluated using the Greenness Evaluation Metric for Analytical Methods (GEMAM), an assessment framework aligned with the core principles of Green Chemistry. GEMAM provides a holistic appraisal of analytical procedures by examining key parameters such as sample handling, chemical inputs, methodological efficiency, instrumental requirements, waste production, and occupational safety. The resulting GEMAM profile (Figure 9) indicates that the proposed platform exhibits a strong environmental performance, particularly with respect to minimal reagent usage, low waste output, energy-efficient instrumentation, and enhanced operator safety.

ARTICLE IN PRESS

The favorable sustainability score can be largely attributed to the streamlined analytical workflow, which requires only the simple dissolution of the analyte in a limited amount of ethanol followed by dilution in an aqueous buffer, eliminating the need for extraction, derivatization, or other resource-intensive pretreatment steps. The exclusive reliance on low-toxicity solvents, combined with the small analytical volume (10 mL per measurement), substantially limits solvent consumption and chemical waste. In addition, the potentiometric technique operates with low energy demand and utilizes compact, reusable equipment, further reinforcing its eco-friendly character. The absence of hazardous chemicals, extreme operating conditions, or specialized radiation sources ensures safe handling and routine laboratory implementation [40]. While the GEMAM analysis reflects a slightly elevated contribution from the sample-related criterion due to off-line sample preparation, this factor represents practical laboratory constraints rather than intrinsic methodological drawbacks. Importantly, it does not detract from the overall green profile of the method. The achieved GEMAM score of 6.345 underscores that the Fe/N-Gr-based sensor offers a sustainable, economical, and environmentally responsible alternative for the determination of APRE in pharmaceutical formulations and biological matrices, outperforming conventional chromatographic approaches in terms of resource efficiency and environmental impact.

ARTICLE IN PRESS

ARTICLE IN PRESS

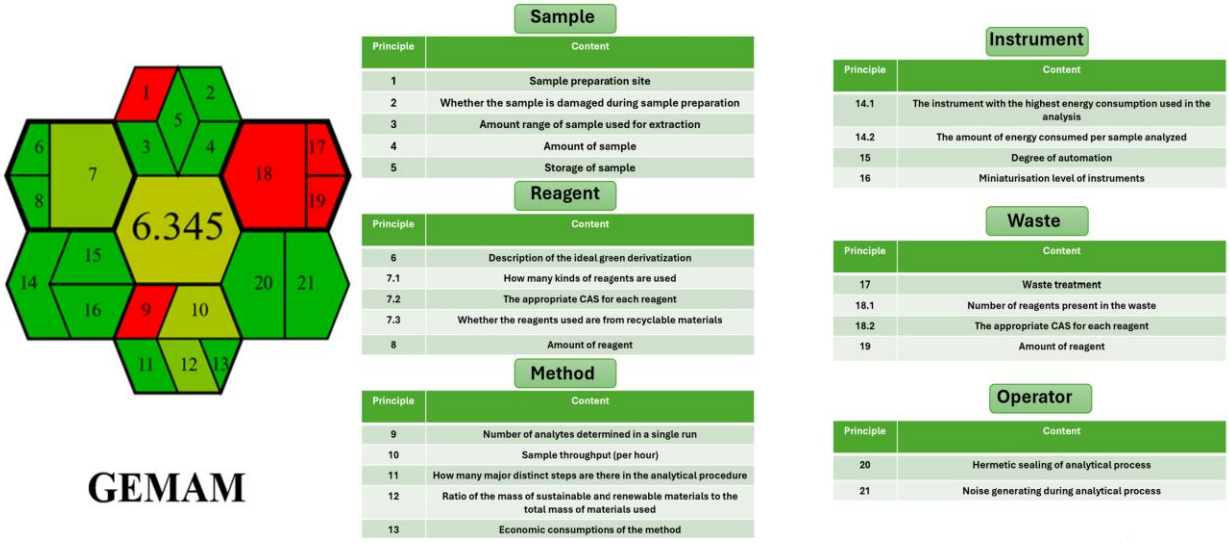


Figure 9. Comprehensive assessment of the analytical greenness of the developed method using the GEMAM framework.

The environmental friendliness of the proposed electrochemical method was assessed using the AGREE metric, which evaluates analytical procedures based on the 12 principles of Green Analytical Chemistry (GAC). This tool provides a quantitative sustainability score ranging from 0 to 1, where values closer to 1 indicate a more environmentally benign method. In this study, the developed procedure achieved an AGREE score of 0.67 (Figure 10), indicating a relatively good green profile. This result reflects advantages such as reduced energy requirements, limited use of hazardous reagents, and overall environmentally conscious experimental design. Nevertheless, certain limitations remain, including the absence of full automation and limited integration of renewable resources. Although the obtained score demonstrates satisfactory sustainability, further optimization could be considered to improve the overall green performance of the method and move closer to ideal GAC compliance.

ARTICLE IN PRESS

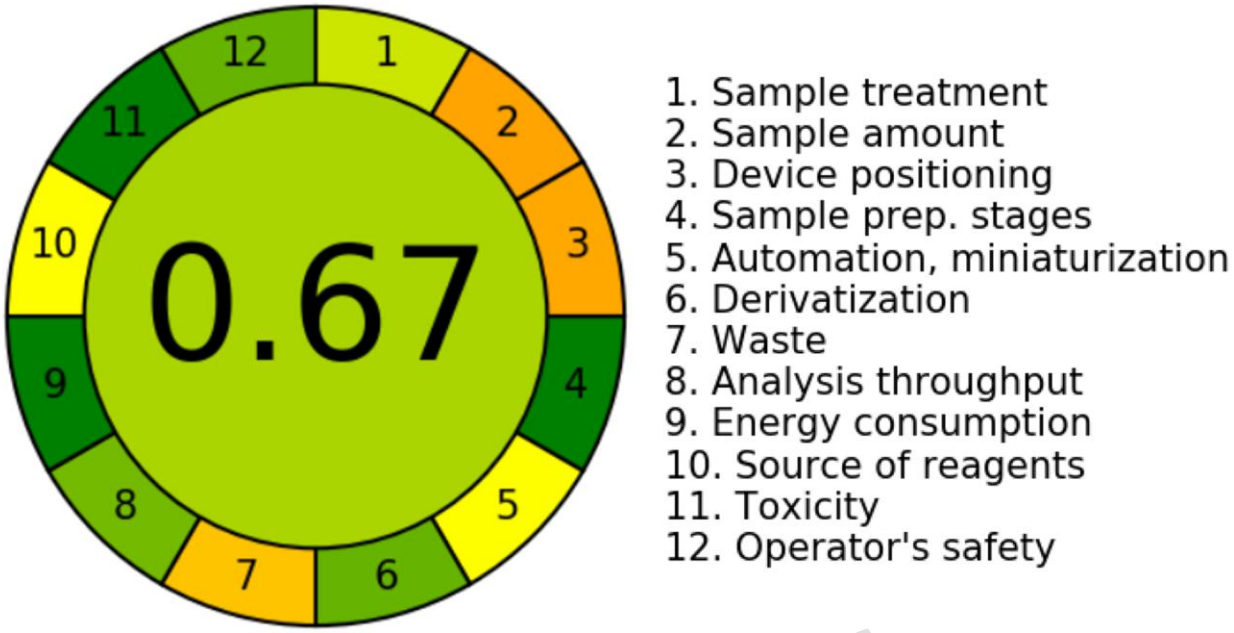


Figure 10. Comprehensive assessment of the analytical greenness of the developed method using the AGREE framework.

The Blue Applicability Grade Index (BAGI) was employed to systematically evaluate the operational suitability and real-world feasibility of the proposed analytical approach. This assessment framework provides both graphical and numerical outputs, where the central value in the asteroid-shaped diagram represents the overall BAGI score, while the surrounding color-coded segments reflect compliance with individual criteria based on blue tonal variations. According to the BAGI methodology, dark blue indicates high compliance, blue represents medium compliance, light blue denotes low compliance, and white corresponds to non-fulfilled criteria. The overall score ranges from 25 to 100, where 25 represents the lowest method applicability, and 100 indicates excellent performance, with values above 60 generally considered acceptable for practical applications [41]. When applied to the developed method, the BAGI evaluation yielded a score of 72.5

ARTICLE IN PRESS

(Figure 11), indicating good practical applicability and compliance with the evaluation criteria. This result reflects the favorable operational characteristics of the proposed method, including a simplified workflow, reduced procedural complexity, and suitability for routine analytical use. Consequently, the proposed strategy demonstrates satisfactory robustness and applicability across different analytical settings and sample matrices.

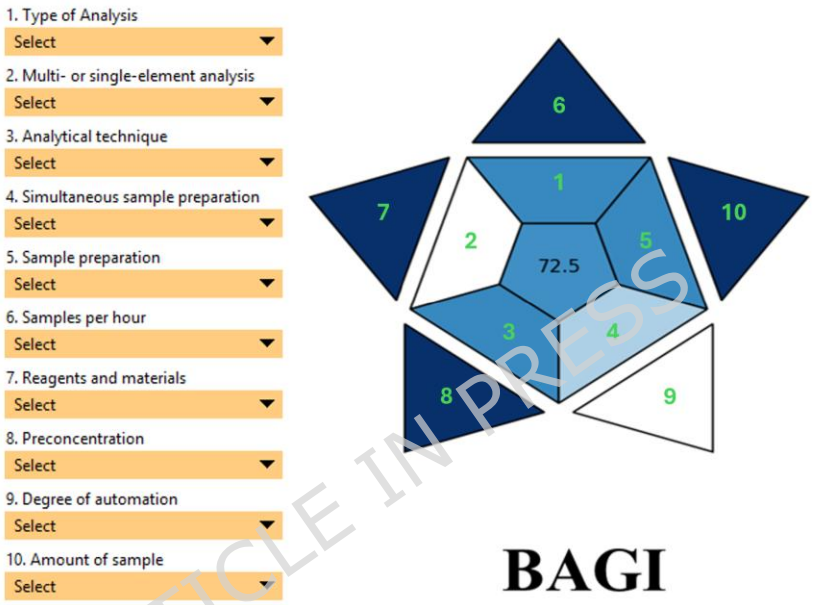


Figure 11. BAGI-based assessment of the analytical blueness of the developed method.

4. Conclusion

In this work, a Fe/N-Gr nanocomposite-modified GCE was developed as an electrochemical sensing platform for the determination of APRE. Based on the available characterization results, the improved response is mainly associated with the nitrogen-functionalized graphene framework and dispersed mixed-valence FeO_x domains. The modified electrode exhibited enhanced electrochemical behavior with improved charge-transfer kinetics and a larger electroactive surface area. These features enabled reliable

ARTICLE IN PRESS

quantification of APRE over a wide linear range with low detection limits. The sensor showed good repeatability, reproducibility, and selectivity under the investigated conditions. The proposed method demonstrates strong compliance with green analytical chemistry principles. It avoids complex sample pretreatment, derivatization, and solvent-intensive extraction steps, thereby reducing reagent consumption and waste generation. The use of small volumes of environmentally benign solvents, together with low energy demand and reusable electrochemical instrumentation, further minimizes environmental impact while ensuring operator safety. The sensor was successfully applied to the determination of APRE in pharmaceutical formulations and biological matrices, with high accuracy and precision. Despite the favorable analytical performance, some limitations should be acknowledged. The applicability of the method was evaluated using synthetic serum and urine samples; therefore, further validation using real clinical samples is required before routine clinical application. In addition, the interference study was limited to selected compounds, and more comprehensive matrix effect investigations are needed. Long-term stability and large-scale reproducibility under extended operational conditions should also be further investigated. Moreover, although the Fe/N-Gr synthesis was conducted under fixed precursor ratios and hydrothermal conditions, quantitative batch-to-batch validation of Fe loading, nitrogen content, and structural consistency was not performed; future studies should address this point using ICP-OES, CHN elemental analysis, and repeated characterization over independently synthesized batches. Overall, the Fe/N-Gr/GCE sensor offers a sensitive, cost-effective, and environmentally sustainable alternative to conventional analytical techniques for routine pharmaceutical quality control and prospective bioanalytical applications.

ARTICLE IN PRESS

Data availability

The datasets generated and/or analysed during the current study are available from the corresponding author on reasonable request.

Funding declaration

N/A

Declaration of generative AI and AI-assisted technologies in the writing process

During the preparation of this work the authors used ChatGPT 5.2 to enhance the readability and language of the manuscript. After using this tool, the authors reviewed and edited the content as required and take full responsibility for the content of the publication.

Reference

1 Kharouf, F. & Gladman, D. D. Advances in the management of psoriatic arthritis in adults. *bmj* **387**, e081860; DOI: 10.1136/bmj-2024-081860 (2024).
2 Chen, L.-g. *et al.* Determination of apremilast in rat plasma by UPLC-MS-MS and its application to a pharmacokinetic study. *J. Chromatogr. Sci* **54**, 1336-1340; DOI: 10.1093/chromsci/bmw072 (2016).
3 Schett, G., Sloan, V. S., Stevens, R. M. & Schafer, P. Apremilast: a novel PDE4 inhibitor in the treatment of autoimmune and inflammatory diseases. *Ther. Adv. Musculoskelet. Dis.* **2**, 271-278; DOI: 10.1177/1759720X10381432 (2010).
4 Xiong, K. *et al.* Identification, characterization and HPLC quantification of impurities in apremilast. *Anal. Methods* **8**, 1889-1897; DOI: 10.1039/C5AY01759A (2016).
5 Bachelez, H. *et al.* Tofacitinib versus etanercept or placebo in moderate-to-severe chronic plaque psoriasis: a phase 3 randomised non-inferiority trial. *Lancet* **386**, 552-56; DOI: 10.1016/S0140-6736(14)62113-9 (2015).
6 Kulkarni, P. & Deshpande, A. Analytical methods for determination of apremilast from bulk, dosage form and biological fluids: A critical review. *Crit. Rev. Anal. Chem.* **51**, 258-267; DOI: 10.1080/10408347.2020.1718481 (2021).
7 Ravisankar, P., Sulthana, M. S. & Babu, P. S. Development and validation of stability-indicating UV spectrophotometric method for determination of Apremilast in bulk and pharmaceutical dosage form. *Indian J. Res. Pharm. Biotechnol.* **5**, 47-53 (2017).

ARTICLE IN PRESS

8 Chaudhari, S. R. & Shirkhedkar, A. A. Design of experiment avenue for development and validation of RP-HPLC-PDA method for determination of apremilast in bulk and in in-house tablet formulation. *J. Anal. Sci. Technol.* **10**, 10; DOI: 10.1186/s40543-019-0170-8 (2019).

9 Nobari, S. G. & Asadpour-Zeynali, K. Magnetite nanoparticles embedded on silver/silver tungstate nano cubes-modified glassy carbon electrode as electrocatalysts for the electrochemical determination of levofloxacin in pharmaceutical formulations and human serum. *Electrochim. Acta.* 559,148579; DOI: 10.1016/j.electacta.2026.148579 (2026).

10 Zhu, C., Yang, G., Li, H., Du, D. & Lin, Y. Electrochemical sensors and biosensors based on nanomaterials and nanostructures. *Anal. Chem.* **87**, 230-249; DOI: 10.1021/ac5039863 (2015).

11 Aftab, R. A., Zaidi, S. & Adim, M. An Overview of Nanomaterial-Modified Electrodes in Biosensing, Pharmaceutical Analysis, and Environmental Monitoring İN *Nanomaterial-Modified Electrodess*, 1-14 (eds Khan, A. A. P., Kulkarni, R. M., Omaish Ansari, M. & Asiri, A. M.); DOI: 10.1007/978-3-031-67176-0_1 (Springer, Cham, 2024).

12 Spinola Machado, S. A. & Cincotto, F. H. Electrochemical methods applied for bioanalysis: differential pulse voltammetry and square wave voltammetry in *Tools and Trends in Bioanalytical Chemistry*, 273-282 (eds Kubota, L. T., da Silva, J. A. F., Sena, M. M. & Alves, W. A.) DOI: 10.1007/978-3-030-82381-8_14 (Springer, Cham, 2022).

13 Öven, E. N. *et al.* Highly sensitive electrochemical determination of cariprazine using a novel Ti3C2@ CoAl2O4 nanocomposite: application to pharmaceutical and biological sample analysis. *Microchim. Acta*. **192**, 248; DOI: 10.1007/s00604-025-07104-1 (2025).

14 Gupta, V. K., Jain, R., Radhapyari, K., Jadon, N. & Agarwal, S. Voltammetric techniques for the assay of pharmaceuticals—a review. *Anal. Biochem.* **408**, 179; DOI:10.1016/j.ab.2010.09.027 (2011).

15 Saputra, H. A. Electrochemical sensors: basic principles, engineering, and state of the art. *Monatsh. Chem.* **154**, 1083-1100; DOI: 10.1007/s00706-023-03113-z (2023).

16 Bouali, W., Genc, A. A., Erk, N., Uzcan, F. & Soylak, M. Highly sensitive electrochemical detection of the tyrosine kinase inhibitor nintedanib using a novel BaTiO□@ MnO□ nanocomposite-based sensor. *Electrochim. Acta*. **539**,147097; DOI: 10.1016/j.electacta.2025.147097 (2025).

17 Sanghavi, B. J., Kalambate, P. K., Karna, S. P. & Srivastava, A. K. Voltammetric determination of sumatriptan based on a graphene/gold nanoparticles/Nafion composite modified glassy carbon electrode. *Talanta* **120**, 1-9; DOI: 10.1016/j.talanta.2013.11.077 (2014).

18 Saini, R., Naaz, F., Bashal, A. H., Pandit, A. H. & Farooq, U. Recent advances in nitrogen-doped graphene-based heterostructures and composites: mechanism and active sites for electrochemical ORR and HER. *Green Chem.* **26**, 57-102; DOI: 10.1039/D3GC03576J (2024).

ARTICLE IN PRESS

19 Zhang, S., Li, M., Li, J., Song, Q. & Liu, X. N-doped carbon-iron heterointerfaces for boosted electrocatalytic active and selective ammonia production. *Proc. Natl. Acad. Sci. U. S. A* **120**, e2207080119; DOI: 10.1073/pnas.2207080119 (2023).

20 Erk, N., Naser, M. & Bouali, W. Ultra-sensitive electrochemical sensor based on tannic acid/iron/titanium oxide for the detection of tyrosine in real biological and food samples. *Microchem. J.* **208**, 112626; DOI:10.1016/j.microc.2024.1126 (2025).

21 Desai, P. B. & Srivastava, A. K. Adsorptive stripping differential pulse voltammetric determination of metoprolol at Nafion-CNT-nano-composite film sensor. *Sens. Actuators B: Chem.* **176**, 632-638; DOI: 10.1016/j.snb.2012.10.073 (2013).

22 Bhakta, A. K. *et al.* Iron nanoparticles decorated multi-wall carbon nanotubes modified carbon paste electrode as an electrochemical sensor for the simultaneous determination of uric acid in the presence of ascorbic acid, dopamine and l-tyrosine. *Mater. Sci. Eng. C.* **57**, 328-337; DOI: 10.1016/j.msec.2015.08.003 (2015).

23 D'Souza, O. J. *et al.* A multi-walled carbon nanotube/poly-2, 6-dichlorophenolindophenol film modified carbon paste electrode for the amperometric determination of l-tyrosine. *RSC Adv.* **5**, 91472-91481; DOI: 10.1039/C5RA18329D (2015).

24 Manasa, G., Raj, C., Satpati, A. K. & Mascarenhas, R. J. S (O) MWCNT/modified carbon paste-A non-enzymatic amperometric sensor for direct determination of 6-mercaptopurine in biological fluids. *Electroanal.* **32**, 2431-2441; DOI: 10.1002/elan.202060049 (2020).

25 Goodrum, R., Weldekidan, H., Li, H., Mohanty, A. K. & Misra, M. Graphene-based nanostructures from green processes and their applications in biomedical sensors. *Adv. Ind. Eng. Polym. Res.* **7**, 37-53; DOI: 10.1016/j.aiepr.2023.03.001 (2024).

26 Baez, D. F. *et al.* Graphene-based sensors for small molecule determination in real samples. *Microchem. J.***167**, 106303; DOI: 10.1016/j.microc.2021.106303 (2021).

27 Hummers Jr, W. S. & Offeman, R. E. Preparation of graphitic oxide. *J. Am. Chem. Soc.* **80**, 1339-1339 (1958).

28 Karaman, C., Bengoa, L. N., Gil, R. M. G. & Gomez-Romero, P. Quinone Quest: Unraveling electrochemical performance in quinone-anchored 3D graphene architectures for high-energy supercapacitors. *Electrochim. Acta.* **512**, 145414; DOI: 10.1016/j.electacta.2024.145414 (2025).

29 Zhu, Y. *et al.* An improved Hummers method to synthesize graphene oxide using much less concentrated sulfuric acid. *Chin. Chem. Lett.* **33**, 4541-4544; DOI: 10.1016/j.cclet.2022.01.060 (2022).

30 Krishnamoorthy, K., Veerapandian, M., Yun, K. & Kim, S.-J. The chemical and structural analysis of graphene oxide with different degrees of oxidation. *Carbon* **53**, 38-49; DOI: 10.1016/j.carbon.2012.10.013 (2013).

31 Stobinski, L. *et al.* Graphene oxide and reduced graphene oxide studied by the XRD, TEM and electron spectroscopy methods. *J. Electron Spectrosc. Relat. Phenom.* **195**, 145-154; DOI: 10.1016/j.elspec.2014.07.003 (2014).

ARTICLE IN PRESS

32 Wachs, I. E. & Bañares, M. A. *Springer handbook of advanced catalyst characterization*. (Springer Nature, 2023).

33 He, K., Chen, N., Wang, C., Wei, L. & Chen, J. Method for determining crystal grain size by x-ray diffraction. *Cryst. Res. Technol.* **53**, 1700157; DOI: 10.1002/crat.201700157 (2018).

34 Romero-Orellana, L. A. *et al.* Synergistic metal-carbon interactions in Fe 3 O 4/N-MWCNT composites for electro-Fenton processes. *RSC Adv.* **15**, 46367-46379; 10.1039/d5ra06118k (2025).

35 Leśniewski, B., Kotula, M., Kubiak, A. & Pajewska-Szmyt, M. Thermostability of Selected Biological Materials. *Lett. Appl. NanoBioScience* **12**, 2284-6808; DOI: 10.33263/LIANBS123.088 (2022)

36 Norizan, M. N., Abdan, K., Salit, M. S. & Mohamed, R. Physical, mechanical and thermal properties of sugar palm yarn fibre loading on reinforced unsaturated polyester composites. *J.Phys.Sci.* **28**, 115-136; DOI: 10.21315/jps2017.28.3.8 (2017).

37 Cheng, W., Tang, K., Qi, Y., Sheng, J. & Liu, Z. One-step synthesis of superparamagnetic monodisperse porous Fe 3 O 4 hollow and core-shell spheres. *J.Mat. Chem.* **20**, 1799-1805; DOI: 10.1039/B919164J (2010).

38 Naser, M. *et al.* Experimental and theoretical studies on Ritlecitinib: A new electrochemical sensor, DFT, and Molecular Docking. *Electrochim. Acta*. **537**,146885; DOI: 10.1016/j.electacta.2025.146885 (2025).

39 Ravisankar, P., Sulthana, M. S. & Babu, P. S. Development and validation of stability-indicating UV spectrophotometric method for determination of Apremilast in bulk and pharmaceutical dosage form. *Ind. J. Res. Pharm. Biotechnol.* **5**, 47 (2017).

40 Xin, T. *et al.* Greenness evaluation metric for analytical methods and software. *J. Pharma. Anal.*, **15**,101202; DOI: 10.1016/j.jpha.2025.101202 (2025).

41 Manousi, N., Wojnowski, W., Płotka-Wasylka, J. & Samanidou, V. Blue applicability grade index (BAGI) and software: a new tool for the evaluation of method practicality. *Green Chem.* **25**, 7598-7604; DOI: 10.1039/D3GC02347Hß (2023).

ARTICLE IN PRESS